Design, microfabrication, and analysis of micrometer-sized cylindrical ion trap arrays

D. Cruz, J. P. Chang, M. Fico, A. J. Guymon, D. E. Austin, and M. G. Blain

Citation: Review of Scientific Instruments **78**, 015107 (2007); doi: 10.1063/1.2403840
View online: https://doi.org/10.1063/1.2403840
View Table of Contents: http://aip.scitation.org/toc/rsi/78/1
Published by the American Institute of Physics

Design, microfabrication, and analysis of micrometer-sized cylindrical ion trap arrays

D. Cruz
University of California, Los Angeles, Los Angeles, California 90095 and Sandia National Laboratories, Albuquerque, New Mexico 87185

J. P. Chang
University of California, Los Angeles, Los Angeles, California 90095

M. Fico and A. J. Guymon
Department of Chemistry, Purdue University, West Lafayette, Indiana 47907

D. E. Austin[a] and M. G. Blain[b]
Sandia National Laboratories, Albuquerque, New Mexico 87185

(Received 28 July 2006; accepted 7 November 2006; published online 17 January 2007)

A description of the design and microfabrication of arrays of micrometer-scale cylindrical ion traps is offered. Electrical characterization and initial ion trapping experiments with a massively parallel array of 5 μm internal radius (r_0) sized cylindrical ion traps (CITs) are also described. The ion trap, materials, and design are presented and shown to be critical in achieving minimal trapping potential while maintaining minimal power consumption. The ion traps, fabricated with metal electrodes, have inner radii of 1, 2, 5, and 10 μm and range from 5 to 24 μm in height. The electrical characteristics of packaged ion trap arrays were measured with a vector network analyzer. The testing focused on trapping toluene (C_7H_8), mass 91, 92, or 93 amu, in the 5 μm sized CITs. Ions were formed via electron impact ionization and were ejected by turning off the rf voltage applied to the ring electrode; a current signal was collected at this time. Optimum ionization and trapping conditions, such as a sufficient pseudopotential well and high ionization to ion loss rate ratio (as determined by simulation), proved to be difficult to establish due to the high device capacitance and the presence of exposed dielectric material in the trapping region. However, evidence was obtained suggesting the trapping of ions in 1%–15% of the traps in the array. These first tests on micrometer-scale CITs indicated the necessary materials and device design modifications for realizing ultrasmall and low power ion traps. © *2007 American Institute of Physics.*
[DOI: 10.1063/1.2403840]

I. INTRODUCTION

The ion trap has become an essential tool in several areas of physical science, including mass spectrometry,[1,2] atomic frequency standards,[3] studies of fundamental quantum dynamics,[4] and quantum information science.[5] Many of these applications would benefit from miniaturized ion trap dimensions several orders of magnitude below the current centimeter and millimeter scales. The design considerations of micrometer-sized cylindrical ion traps (CITs) for mass spectrometry applications were previously described.[6] Moreover, the field emission characteristics of the ion trap device to determine maximum voltage operation limits have been studied.[7] Although the application of the micrometer-scale ion traps described herein focuses on mass spectrometry applications, the method of fabrication can be adapted and is useful to other applications. This article deals specifically with the design, microfabrication, electrical characterization, and analysis of arrays of micrometer-sized cylindrical ion traps.

The miniaturization of the ion trap to the millimeter scale has been investigated, and transportable ion trap mass spectrometers have been described.[8–12] Linear Paul traps have been investigated[13,14] and provide simple construction while maintaining minimal distortion of the radio-frequency field. Microfabricated cylindrical traps with polysilicon electrodes insulated from each other by silicon dioxide dielectric of radius 20 μm also have been recently fabricated and tested.[15] In this work, we describe the design and fabrication of cylindrical ion traps with metal electrodes and air gap separation between the electrodes. The design, simulation, microfabrication, and electrical parametric testing of ion trap cylinders with radii of 1, 2, 5, and 10 μm and the operational testing of 5 μm radius traps are discussed in detail.

Conventional ion traps consist of three hyperbolic electrodes, a ring electrode and two end cap electrodes, which define a quadrupolar field when a time varying rf potential is applied to the ring electrode. Numerous reviews have appeared that describe the theory of rf ion traps used for ion

[a]Present address: Brigham Young University, Provo., UT 84602.
[b]Author to whom correspondence should be addressed; electronic mail: blainmg@sandia.gov

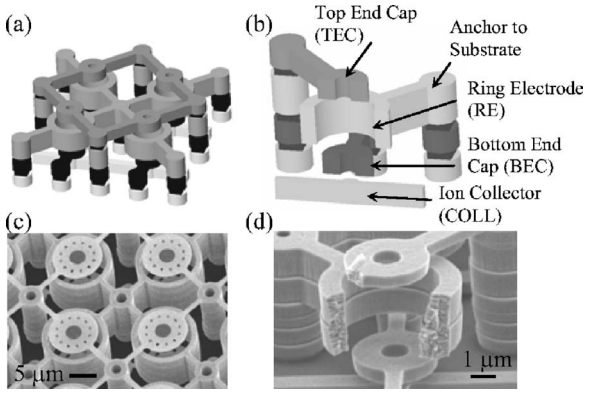

FIG. 1. (a) A unit cell of a hcp array of overhung ion traps. (b) A cross-sectional perspective of the overhung ion trap design. The trap consists of two end cap electrodes, a ring electrode, and an ion collector. All electrodes are anchored to the substrate by vias.

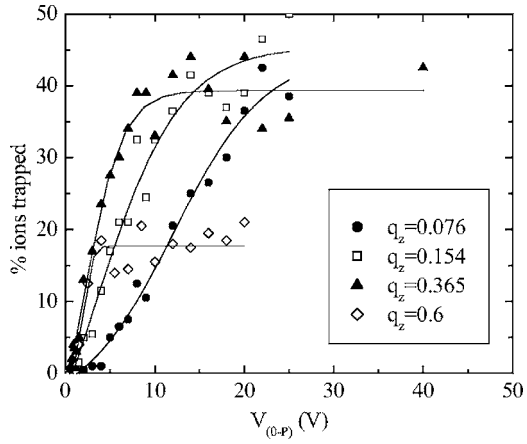

FIG. 2. Simulation of the ion trapping efficiency at 1 GHz as a function of voltage and several stability parameter (q_z) values for the r_0=1 μm sized ion trap [Fig. 1 (a)]. The trapping efficiency saturates as the voltage is increased, allowing the trap operation to be in the range of 5–20 V.

storage and mass spectrometry.[2] In general, ions are either radially or axially trapped in a quadrupolar field at a given moment in time. Although hyperbolic electrodes define a linear order field with minimal distortions, i.e., less higher order components, they are not amenable to high precision machining. Alternatively, cylindrical ring electrodes are used. These electrodes provide a good approximation of the quadrupole field and are more easily machined. Although CITs contain higher order fields, they are still quite adequate as mass analyzers in mass spectrometers.[16,17]

A trap electrode fabrication method based on microelectromechanical systems (MEMS) and integrated circuit (IC) processing techniques is presented. The objective is to create a micrometer-scale ion trap operating at low rf voltage which allows for monolithic integration with solid-state electronics. Moreover, it is argued that the method of fabrication is critically important and that the method presented here is versatile, so that it may be used by different sectors of the ion trap community. Miniaturizing ion traps by several orders of magnitude yields new challenges not encountered in the macroscale. Although the trapping mechanism and trap operation remain the same, as elucidated by simulations, the unique mechanical and electrical characteristics of the micrometer-scale structures are important factors in the performance of the traps.

The contribution of this work is to describe the design, fabrication, electrical properties, and the testing of the smallest cylindrical ion traps and largest array of traps attempted to date. It is hoped that this initial work will lead to further advances in the field of micrometer-sized ion traps.

II. rf TRAP OPERATION

Some basic operational aspects of cylindrical ion traps are reviewed. Figure 1 depicts our designed and fabricated cylindrical ion traps, arrayed to achieve large numbers of traps. rf voltage is applied to the ring electrode, while static voltages are applied to the end caps. In this case, the trap operation is governed by the Mathieu stability equation, the solution of which gives

$$\frac{m}{z} = \frac{8V_{0-P}}{q_z(r_0^2 + 2z_0^2)\Omega^2}, \tag{1}$$

where m/z represents the mass to charge ratio of the species that is trapped, V_{0-P} is the applied rf voltage from 0 to peak, Ω is the radial frequency $(2\pi f)$, r_0 is the inner radius of the ring electrode, and z_0 is the half-height of the trap. The value of q_z determines whether ion trajectories are stable and depends on r, z, Ω, and V_{0-P}. For an ideal (i.e., hyperbolic) trap $q<0.908$ describes stable ion trajectories. Additionally, z_0 is typically related to r_0 by

$$r_0^2 = 2z_0^2. \tag{2}$$

Therefore, as the size of the trap decreases, ions of higher mass may be trapped. Adjustments for smaller masses can be made by operating at higher frequencies and smaller voltages. However, the voltage may not be chosen to be arbitrarily small. The voltage along with q_z can be used to determine the trapping pseudopotential well depth, D_z. If ions have energy greater than the potential well, they will not be trapped. The trap depth can be estimated by[18]

$$D_z = \frac{V_{\text{eff}}}{8q_z}, \quad \text{where } V_{\text{eff}} = 0.55V_{0-P} \quad \text{for } q_z \leq 0.4. \tag{3}$$

Detailed simulations[19] of ion behavior in micrometer-sized cylindrical ion traps were performed using SIMION.[20] The effects of ion and neutral temperature, the pressure and nature of cooling gas, ion mass, trap voltage and frequency, space charge, fabrication defects, and other parameters on the ability of micrometer-sized traps to store ions were analyzed. Anharmonic field effects due to space charge result in a trapping limit of a single ion per trap. For successful long-term trapping, this ion must have energy below or equal to the pseudopotential well throughout its trapped lifetime and a "stable" trajectory, i.e., one which will not lead it to hit an electrode. Simulation of ion trapping as a function of the applied rf voltage for different q_z values in a 1 μm internal radius ion trap, Fig. 1(e), is shown in Fig. 2. The ion of interest is toluene with m/z=91, 92, or 93. Ions were considered to be trapped if they remained in the trap for

2000 cycles (2 μs at 1 GHz drive frequency), and the ion trapping efficiency is defined as the percentage of ions trapped among all sampled ions. A saturation of the ion trapping efficiency is seen with increasing voltage, in the range of 5–20 V, meaning that trapping does not arbitrarily increase with an increase in the rf voltage applied to the ring electrode. Note that lines are added in the figure to guide the eyes and do not represent a fit.

For a given q_z value, increasing the voltage beyond the saturation point does not increase the trapping efficiency. Thus it is predicted that the micrometer-scale ion traps will operate at hundreds of megahertz with operating voltages in the range of 5–20 V. In the following sections the materials amenable to the microfabrication of the ion traps and the consequent design arising from microfabrication restrictions are described.

III. CYLINDRICAL ION TRAP DESIGN

While cylindrical electrodes are a simplification of hyperbolic electrodes, their design and microfabrication are not trivial. The electrodes must be able to provide a sufficient trap potential depth, as well as minimize higher order fields.[21,22] In an ideal hyperbolic trap of similar nature, the number of trapped ions ($N_{\max}$) based on space charge considerations is estimated using the Dehmelt space charge limit:[18]

$$N_{\max} = \frac{3}{16\pi}\frac{V_{0-P}^2}{mz_0^4\Omega^2}. \tag{4}$$

Equation (4) can be used to approximate the maximum number of ions trapped. A single trap of radius of 1 μm is able to trap at most about 100 ions. However, if 10^6 traps are arrayed in parallel, about 1×10^8 ions could be trapped. Thus, a massively parallel array of traps would have a trapping capacity comparable to that of a single $r_0=1$ cm sized trap. The micrometer-sized trap would have the advantage of operating at much lower voltages and theoretically lead to less power consumption. Higher pressure operation would also be expected.

Although the arrangement of the electrodes is predetermined, i.e., a cylinder, the shape and dimensions of the electrodes yield a wide variety of electrical characteristics. The capacitance, inductance, and resistance of the structure determine the resonant frequency and the power delivered to the structure and are therefore important characteristics to be considered. If the power consumption of the structure is too high, the benefits achieved by the miniaturization of the trap are lost.

First, we consider the capacitance of the designed CITs. The ion trap structure is, by nature, a parallel plate capacitor as it consists of overlapping metal electrodes, thus the capacitance (C) is given by the product of dielectric permittivity and the overlap area of the plates divided by the distance separating the plates. For a 1 cm^2 area (the area need to array 10^6 traps) separated by a 0.5 μm gap, where the dielectric is silicon dioxide (SiO_2), the capacitance is approximately 8 nF. If vacuum or free space is the dielectric, the capacitance is decreased to 2 nF. This capacitance can be further decreased if the overlap area of the electrodes is reduced. Hence, for CITs with $r_0=1$ μm, separated by a distance of 0.4 μm and end cap to ring electrode (vertical) distance of 0.2 μm, the capacitances for an array of 2×10^6 CITs is estimated to be ~70 pF. From this, the power can be estimated from the reactive capacitance X_c of the structure to be $P=V_{0-P}^2/X_c=V_{0-P}^2\Omega C$. Therefore, if the traps are operated at a frequency of 1 GHz and a zero-to-peak voltage of $10V_{0-P}$, the estimated power consumption is approximately 10 W based on the capacitance consideration alone.

The capacitance consideration led to the design of the overhung structures, and Fig. 1(a) depicts a unit cell of an array consisting of four traps. Each trap consists of two end cap electrodes (a top end cap designated TEC and a bottom end cap designated BEC), one ring electrode (designated RE), and an ion collector plate (designated COLL). In this design, the metal layers are independently anchored to the substrate by dedicated vias. The outer radius of the end caps is less than or equal to that of the ring electrode. Overlap between electrodes only occurs where their support struts overlap with the previous electrodes. Although this design greatly reduces the overlap between the electrodes, vias must be patterned. This increases the number of photomasks required for building the structure since it is not a blanket dielectric film that is deposited in between electrodes as in the aforementioned designs, and each electrode is dependent on the previous layers for anchoring and support. Figures 1(c) and 1(d) show the cross-sectional scanning electron microscopy (SEM) images of the fabricated cylindrical ion trap array.

In addition to the capacitance consideration, a good rf conductor is desired for the arrays of micron-scale cylindrical ion traps. Tungsten was determined to be the best material in comparison with copper, aluminum, gold, and silicon based on its resistivity (5.39 $\mu\Omega$ cm), skin depths at high and low frequencies (11.68 μm at 100 MHz and 3.6 μm at 1 GHz), thermal conductivity (1.74 W/cm K), melting temperature (3414 °C), and the available method of fabrication.

Utilizing tungsten, the resistance of the metal structure can be incorporated into the power calculation, in which the average power into a general ac circuit is given by P_{av}:

$$P_{\text{av}} = \tfrac{1}{2}V_{0-P}I\cos\phi. \tag{5}$$

The factor $\cos\phi$ is the power factor of the circuit. For a pure resistance, $\phi=0$ and $\cos\phi=1$. For a pure capacitance or inductance, $\phi=\pm90°$, $\cos\phi=0$, and $P_{\text{av}}=0$. For a L-R-C circuit, the power factor is equal to R/Z, where Z is the impedance, and for a series L-R-C circuit, the magnitude of Z is given by

$$Z = \sqrt{R^2 + (X_L - X_C)^2}. \tag{6}$$

Thus the average power into the trap at a frequency of 1 GHz operated at $10V_{0-P}$ is estimated to be 16 W. The power calculation could be more accurate if the inductance could be estimated from first principles; however, this presents a challenge because only the single coil model was available for the inductance calculation.

In order to electrically characterize the arrays of ion traps, electrical test structures were designed and fabricated

(as chip-based devices separate from the ion trap chip that was tested) in order to determine the ion trap's electrical characteristics. These structures included the S_{11} and S_{12} scattering parameter structures. In this work, S_{11} refers to a trap array in which there is only one port to which voltage is applied and taken away. S_{12} refers to a microwave network into which there is one port in which power can be fed and a second port in which power can be taken away. The real and imaginary parts, or the modulus and the phase angle, of each of these two scattering parameters determine the impedance. Specifically, the incoming and outgoing wave quantities are assembled into n-vectors $\mathbf{A}$ and $\mathbf{B}$, and $\mathbf{B}=S\mathbf{A}$, where S is an $n\times n$ square scattering matrix:

$$\begin{bmatrix} b_1 \\ b_2 \end{bmatrix} = \begin{bmatrix} S_{11} & S_{12} \\ S_{21} & S_{22} \end{bmatrix} \begin{bmatrix} a_1 \\ a_2 \end{bmatrix}. \tag{7}$$

These four S parameters are complex quantities and contain eight separate numbers: the real and imaginary parts, or the modulus and the phase angle. It is clear that the magnitude of S_{11} and S_{21} determines how the input power splits between the possible output paths.[23] Therefore, these S parameters help determine a match to the input wave.

IV. FABRICATION

The ion traps were microfabricated using a molded tungsten fabrication sequence, a process that has been used for the fabrication of metal MEMS devices such as photonic crystal lattices.[24] Other electrode materials were considered, for example, copper and aluminum; however, both of these were deemed not suitable because of the poor electrode profiles that result. The molded tungsten process sequence, sometimes referred to as a "damascene" process, begins with silicon dioxide deposition using a tetraethylorthosilicate (TEOS) precursor in a plasma enhanced chemical vapor deposition (PECVD) reactor. The SiO_2 was patterned and then etched to form trenches using a CHF_3 plasma. After a 25 nm adhesion layer of sputtered TiN, tungsten was deposited, overfilling the trench features previously etched in the silicon dioxide mold, via chemical vapor deposition (CVD) in a cold wall reactor, using tungsten hexafluoride (WF_6) as the precursor at approximately 400 °C. Next, the tungsten was planarized to the oxide thickness (thereby removing the W on top of the SiO_2 and leaving W in the trenches) by chemical-mechanical polishing (CMP), using a polyurethane pad and acidic slurry containing an oxidizer and colloidal alumina. This results in a W structural layer that is rectangular in cross section and having 25 nm of TiN on the sides and bottom. This process is repeated until all electrode and via levels had been made. Approximately 8000 Å of aluminum was sputter deposited and then patterned via plasma etching to make electrical contact pads. The completed W trap electrode structures were released in a hydrofluoric (HF) acid solution. Preliminary releases were performed in solutions containing a 49% HF solution diluted with one part water ($HF:H_2O$ 1:1). The HF solution was further buffered to prevent attack to the Al defining the electrical pads.

The ion trap chips were packaged in rf quad-flat-pack packages. These packages have a cavity well and straight leads protruding from all four sides. The packages were made of glass with 20% Al, and the leads were made of an F-15 alloy. The dice were attached to the bottom of the packages using a nonconductive cyanate ester (JM7000©), and electrical connections were made to the leads from bond pads on the dice through low inductance gold ribbon bonds. The trap chips were wired so that they retained a ground-signal-ground configuration. The package leads were soldered onto Duroid® boards having 50 Ω microstrip lines tapered into 50 Ω coplanar waveguides (CPWs) and SMA connectors. This board is fitted to the flange of the vacuum chamber. Coaxial cables were used to connect the SMA connectors to vacuum electrical feedthroughs.

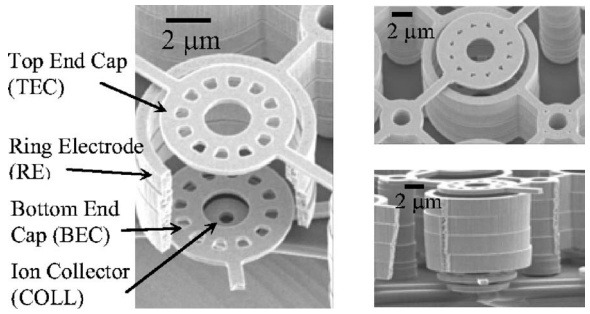

FIG. 3. Scanning electron microscopy micrographs of the microfabricated $r_0=5$ μm CIT: (a) a cross-sectional perspective view showing various electrodes, (b) top view of an array, and (c) the side view showing the electrodes.

V. ELECTRICAL CHARACTERISTICS

The devices characterized in this work were arrays of micrometer-scale ion traps,[6] with inner radii of 1, 2, 5, and 10 μm. Scanning electron micrographs of the $r_0=5$ μm ion trap and ion trap array, Fig. 3(a), show in a perspective view the electrodes and the traps arranged in a large two-dimensional array. The electrodes are vertically separated by a 0.5 μm gap and horizontally separated by 4.5 μm. Common anchor points of adjacent elements allow for the entire array of traps to be operated in parallel, as seen in Fig. 3(b), while Fig. 3(c) depicts the side view of the fabricated ion trap. Anchor points of differing electrodes are separated by 8 μm or more, and all anchors are landed on a dielectric stack of 800 nm of silicon nitride on 630 nm of silicon dioxide on the silicon substrate. Although the trap electrodes are isolated from the substrate by the dielectric stack, they are capacitively coupled to each other through the substrate. This accounts for approximately 30% of the measured capacitance. However, the use of high resistivity silicon should substantially alleviate this coupling.[25–27]

Before testing the ion trap array for trapping, the electrical characteristics of the packaged and nonpackaged ion trap arrays were determined. The trap electrodes act as electrical circuit components such as capacitors, resistors, and/or inductors. The general circuit description of the ion trap array is a line terminated at an arbitrary load, as shown in Fig. 4. The impedance of the load, in this case the ion trap array, must be determined for shaping how power and voltage are

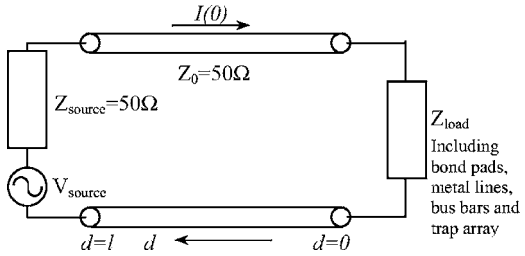

FIG. 4. A schematic diagram of a circuit for a wave traveling through a line of length L, and being terminated at an arbitrary load impedance. Typically the line and source impedances are 50 Ω.

delivered to the ring electrode. The impedance of the ion trap array can be determined by measuring the scattering parameters, S_{11} and S_{12}.

The electrical characteristics of the ion trap arrays were measured using a Wiltron 360B vector network analyzer. Measurements of the trap arrays (not packaged) with 20 736 ion traps of radius 5 μm (referred to as r_0=5 μm "medium" sized array) were made to determine die level properties. Figure 5 shows the measured S_{11} real and imaginary parts from 40 MHz to 4.04 GHz, along with the fitted series resistance, inductance, and capacitance (R-L-C) circuit model. The model was fitted from 40 to 540 MHz and determined a resistance value of 7 Ω, an inductance value of 554 pH, and a capacitance value of 52 pF.

Figure 6 shows the measured S_{11} real and imaginary parts for packaged r_0=5 μm medium sized arrays from 40 MHz to 4.04 GHz. The die level test is shown for reference. The first set of data gives values for the equivalent circuit elements for rf applied to the ring electrode of a packaged ion-trap array, where the TEC, BEC, and COLL were shorted to ground through the package leads. In this case the fitted R-L-C series circuit model yielded a resistance value of 1.77 Ω, an inductance value of 4386 pH, and a capacitance value of 49.6 pF. The second set of data shows results for the packaged part with TEC, BEC, and COLL shorted to ground through their respective pads to the ground ring (at die level).

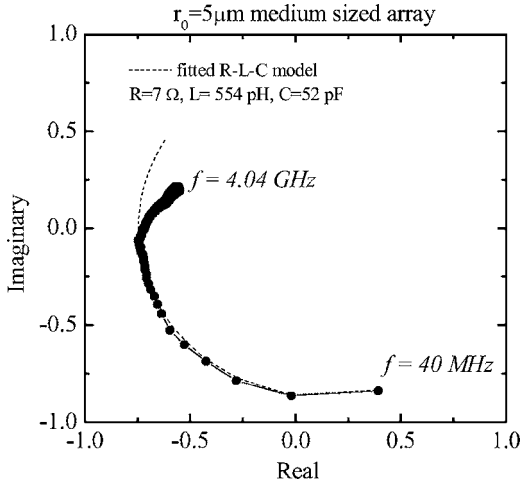

FIG. 5. The measured S_{11} parameters and fitted series R-L-C model for an unpackaged r_0=5 μm medium sized array, using a Wiltron 360B VNA. The fit was good from 40 to 540 MHz, then began to deviate. The fitted parameters were R=7 Ω, L=554 pH, and C=52 pF.

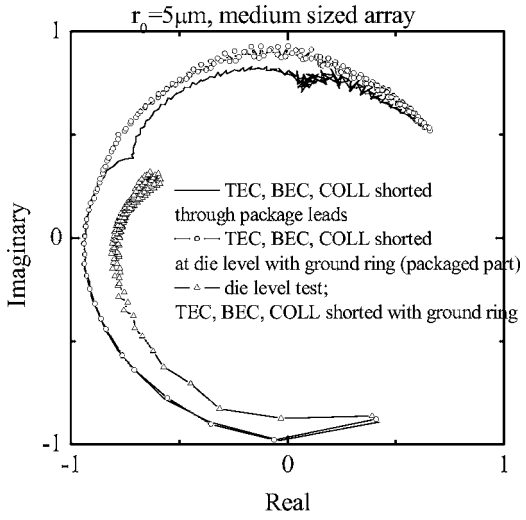

FIG. 6. The measured S_{11} parameters of a packaged r_0=5 μm medium sized array. The measurements were made using a Wiltron 360B VNA. The first set of data shows the packaged part, where the TEC, BEC, and COLL were shorted to ground through the package leads. The second set of data shows the packaged part where the TEC, BEC, and COLL were shorted to ground through their respective pads to the ground ring. The third set of data is the reference showing the results from an unpackaged part, the die level test, where the TEC, BEC, and COLL were shorted to ground through their respective pads to the ground ring.

In this case the fitted series R-L-C circuit model yielded a resistance value of 2.21 Ω, an inductance value of 2096 pH, and a capacitance value of 50 pF. These results show that the package leads contribute approximately 2.3 nH of inductance.

Figure 7(a) shows the schematic of the equivalent series L-R-C circuit for the packaged traps. The majority of the inductance L is due to the package leads, wirebonds, and bus bars in the array. Approximately 550 pH of the inductance

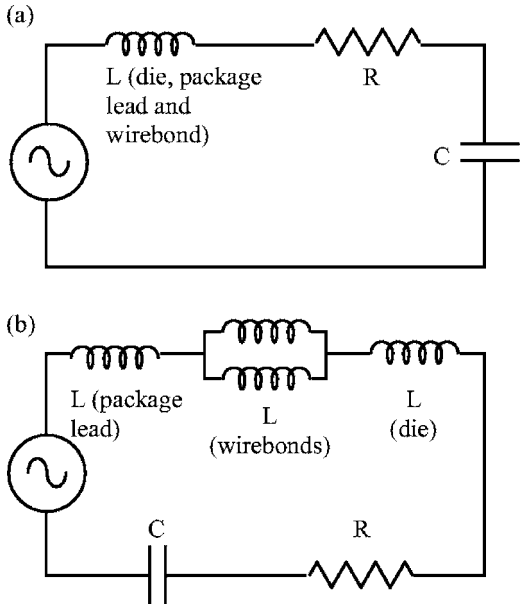

FIG. 7. (a) An equivalent R-L-C circuit of microfabricated and packaged cylindrical ion trap arrays. The inductance is mainly due to the wirebonds used for making electrical connections to packages, the bus bars of the fabricated die, and the package leads. (b) An equivalent R-L-C circuit with the parallel inductance by the addition of wirebonds.

TABLE I. Electrical characteristics of microfabricated cylindrical ion trap arrays.

r_0 (μm)	Array size	R (Ω)	L (pH)	C (pF)	Sum of difference of squares
1	1 073 290	2.18	1646.00	576.00	0.031 70
	217 156	1.74	712.22	120.87	0.001 29
	7 396	8.99	9.99	4.92	0.003 00
2	331 776	1.57	1190.00	399.98	0.013 90
	66 564	1.48	596.80	73.76	0.000 55
	2 304	33.70	9.97	3.44	0.029 80
5	104 976				
	20 736	7.06	554.00	51.60	0.002 80
	784	16.50	99.99	2.83	0.003 00
2 (packaged)	66 564	6.76	3303.00	70.00	1.750 00
5 (packaged)	20 736	1.77	4386.00	49.60	0.006 00

are due to the actual array. The package leads and wirebonds add about 4000 pH of inductance: 2000 pH from the package leads and 2000 pH from the wirebonds. Consequently, it was not possible to externally match the circuit outside the package. Thus, the effective inductance of the packaged trap arrays was reduced by the addition of parallel wirebonds. The new equivalent circuit is seen in Fig. 7(b). Adding parallel wirebonds having equal amounts of inductance reduces the total inductance of the wirebonds by one-half. This overall reduction in inductance leads to a reduction in the reflected power and an increase in the resonant frequency at which the traps can be operated, thereby increasing the required voltage needed to trap ions of a specific mass. The difference in impedance between the packaged array and the 50 Ω transmission line creates a discontinuity of the wave propagation into the device. Ideally, the device would have an impedance of 50 Ω and be matched with the transmission line, with no resulting power loss or standing waves. Too much capacitance, however, precluded matching and power was reflected from the load in the range of 50%–66% of the forward power. The standing wave ratio (SWR) was estimated to be approximately 4, using the following relationship:

$$\mathrm{SWR} = 1 + \frac{\sqrt{P_{\mathrm{ref}}/P_{\mathrm{fwd}}}}{1 - \sqrt{P_{\mathrm{ref}}/P_{\mathrm{fwd}}}}, \tag{8}$$

where P_{ref} is the reflected power at the load and P_{fwd} is the forward power. If P_{ref} is close to 0, then the SWR approaches 1, the desired value. If P_{ref} approaches P_{fwd}, then the SWR approaches infinity, a highly undesirable condition. A SWR of 4 signifies that there was a substantial power reflected at the load. Thus the design of a proper matching circuit is a major challenge. As rf voltage magnitude determines the pseudopotential well depth, a rf voltage $>8V_{0-P}$ on the ring electrode is required for attaining a sufficient trapping potential within the micron-sized ion traps. However, due to the electrical characteristics of these ion trap arrays, as summarized in Table I, it is nearly impossible to form a matching circuit outside the package.

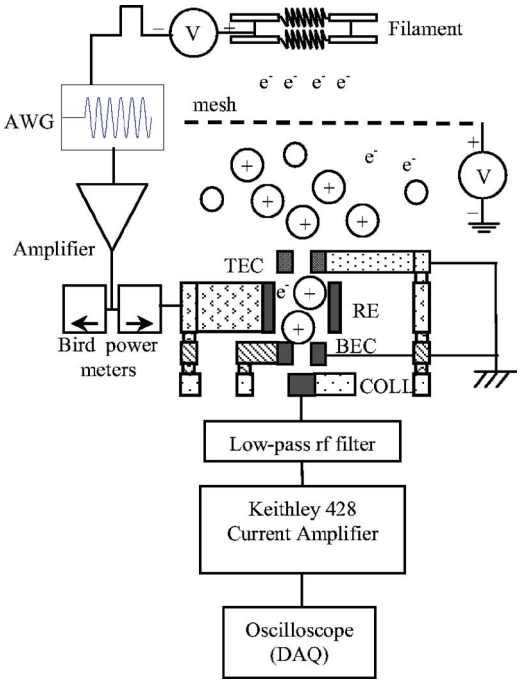

FIG. 8. Test setup for testing the microfabricated cylindrical ion trap arrays. rf voltage was applied to the ring electrode using an arbitrary wave form generator, and signal was measured at the collector electrode. A gated dual rhenium filament provided electrons. Electrons were guided to the traps via a biased mesh. A low pass filter removed rf signal from the collector, and a current to voltage amplifier was implemented for signal amplification. Data acquisition was made by an oscilloscope.

To summarize, the electrical characteristics of the ion trap arrays, including their series resistive, capacitive, and inductive properties, were determined while their field emission properties have been recently published.[7] A further assessment must be made as to the fabrication and features of the device, as their electrical properties present an obstacle in attaining high voltages (>5 V) to the ring electrode. The use of high resistivity silicon was suggested as an alternative to the current fabrication process. However, despite the electrical characteristics, the devices were tested, and their trapping characteristics are discussed in the next section.

VI. TESTING OF MICROMETER-SIZED ION TRAPS

Despite the transmission line discontinuity, various trapping experiments were performed. Figure 8(a) depicts the test setup. Neutrals were ionized by electron impact ionization with two rhenium filaments operated in parallel, yielding electrons with energies of 70 eV. These were gated using the marker function on a Tektronix AWG710 arbitrary wave form generator, and thereby synchronized to the rf signal. The wave form generator AWG710 was also used to simultaneously drive the ring electrode. An amplifier (Amplifier Research) was incorporated for rf voltage amplification, and two Thruline Bird power meters were used to monitor the forward and reflected powers during steady state operation. The top and bottom end caps of the trap arrays were typically grounded. Tungsten collector electrodes on the SiN chip surface below the bottom end cap of each trap were used for ion detection. Since the collector and ring electrodes were capacitively coupled to each other, a low-pass filter was in-

cluded to separate the rf signal picked up by the collector from the ion signal. Because the detected ion current was expected to be on the order of 1–50 nA based on the number of trapped ions, a Keithley 428 current to voltage amplifier was used to increase the output signal and a Tektronix TDS540 oscilloscope was utilized for data acquisition. The chamber was pumped down with a Pfeiffer TMH-071 turbo pump backed with a four stage diaphragm pump. The base pressures ranged from 8×10^{-6} to 1×10^{-5} Torr. The analyte, either toluene or methane, was introduced into the chamber through a Granville-Phillips leak valve, increasing the pressures to the range from 1×10^{-4} to 5×10^{-4} Torr, as monitored by a Granvill-Phillips microion gauge.

Neutral species used for trapping experiments were toluene and methane. Initial trapping experiments used toluene (C_7H_8), mass 92 amu, which has its main ionization peaks at m/z of 91, 92, and 93.[28] Toluene has a relatively high ionization cross section, $\sim15\times10^{-16}$ cm^2,[29] and a low ionization threshold, 8.8 eV.[21] Methane has a higher ionization threshold, 12.6 eV,[21] but lower cross section, 3.5×10^{-16} cm^2.[22]

Experiments were performed at a constant frequency of 200 MHz, and used a standard 30 μs ionization period at V_{0-P}=4 V, followed by 30 μs with only the rf trapping voltage applied, and 1 ms of 0 V dc. The timing sequence is depicted in Figs. 9(a)–9(c) with the resulting current signal at COLL. Figure 9(a) shows the collector signal when there was no toluene present and rf was applied along with electrons. Due to the inverting output of the Keithley 428 amplifier, the electron current is positive and ion current is negative. In Fig. 9(a) during the first 30 μs when the gate was on, more than 50 nA of electron current arrived at the collector, however, the signal was clipped due to the saturation of the amplifier. The current was seen to decrease prior to gate turn off, at which time the signal was dominated by the rf signal. At rf turn off, a large signal increase was again observed. Figure 9(b) depicts the collector signal when 3×10^{-4} Torr of toluene was introduced. A signal in the form of a slight decrease in the measured current was observed, suggesting that ions were formed in the first 30 μs. The rf noise was also decreased, and upon rf turn off, a negative signal was observed, suggesting positive charge being pulsed from the trap array to the collector. The peak of this signal at 61.8 μs was −18.4 nA, while the preceding background amplitude (taken from 56.1 to 60.0 μs) was −17.0 nA, with a standard deviation of 0.1. Under these conditions, mass 91 would be trapped with an estimated q_z value of 0.43. Figure 9(c) depicts the baseline subtracted collector signal [signal in (b)—signal in (a)]. A large spike due to the rf noise was also observed; however, at the rf turn-off event, an isolated ion signal was seen. This signal occurred only when toluene was present.

We note several interesting characteristics of the current measurements in Figs. 9(a) and 9(b). First, although (due to instrumentation) the measured current saturates at ~50 nA during the e^- gate on period, it appears that this current reaches a maximum at a time between 15 and 20 μs and then begins to decrease (this peak is not observed because of the saturation). The decrease occurs prior to, and hence is independent of, the turn off of the ionizing electrons at 30 μs. We believe that this behavior is a result of the negative charging of the silicon nitride surface on which the tungsten trap electrodes are anchored (including the collector from which the current is measured). As the SiN represents over 50% of the area of the ion trap chip being illuminated by the electrons,

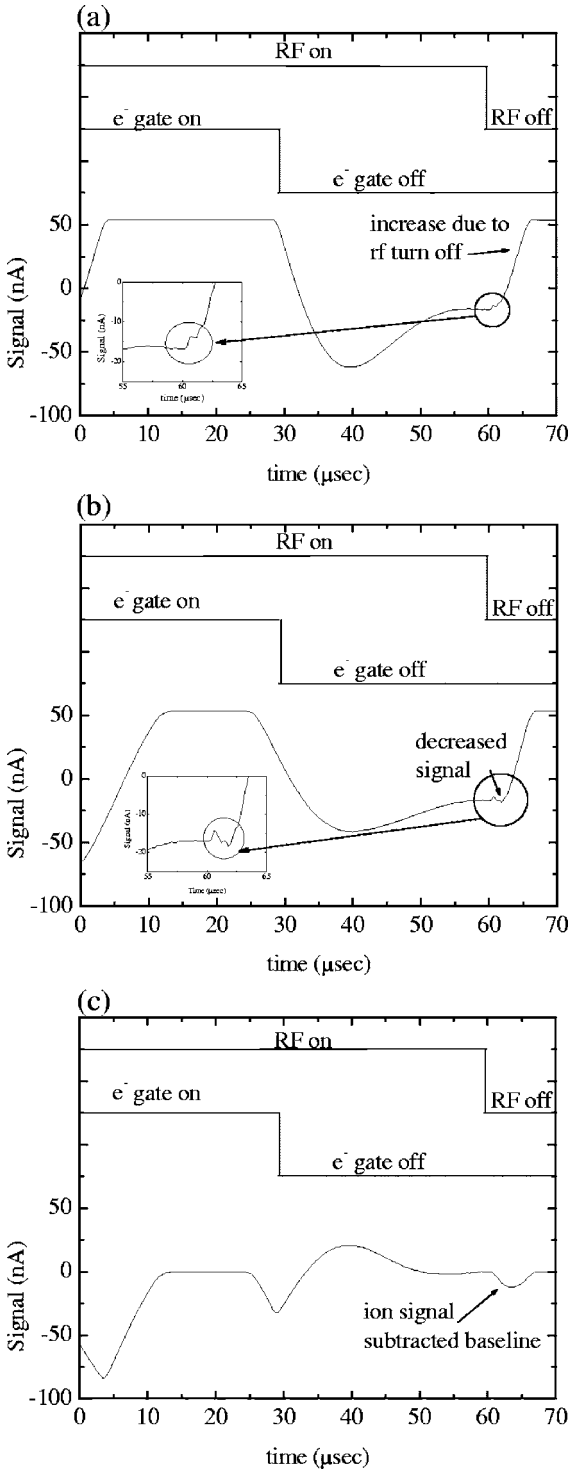

FIG. 9. Signal from the collector electrode of the r_0=5 μm ion trap array: (a) the collector signal without ions, referred to as the baseline in the text; (b) the collector signal when toluene ions were introduced at a partial pressure of 3×10^{-4} Torr; and (c) the collector signal when toluene ions at a partial pressure of 3×10^{-4} Torr were introduced, with the baseline signal subtracted.

we interpret this as evidence that after 15–20 μs, enough negative charge has collected on the SiN to start pinching off the filament current to the collector electrode, and consequently, the signal begins decreasing. We note the same behavior for both the no toluene, background scan shown in Fig. 9(a) and the scan with toluene present in Fig. 9(b). After rf turn off at 60 μs, the collector signal again increases. Since no filament electrons are arriving at the ion trap chip at this time, we interpret this signal increase to be from the discharge of electrons built up on the SiN surface by their migration to the tungsten collector electrode sitting on the SiN.

To confirm whether the background corrected collector signal after baseline subtraction was due to trapped ions, methane ($m/z=16$) was substituted for toluene. Under identical trapping conditions (4 V and 200 MHz) methane is not expected to be trapped, as the estimated q_z value is 2.4, well beyond the stability region. Using methane, both the observed and baseline subtracted signals were similar, however, the toluene signal was greater than the methane signal by about 5 nA, again suggesting that part of the signal is indeed due to the trapped toluene ions. An alternative explanation for the larger signal amplitude for toluene compared to methane is that the rf coupling from RE to COLL upon turn off is larger due the larger dielectric constant of toluene relative to methane (the average electric dipole polarizability for ground state toluene is $\alpha=12.3\times10^{-24}$ cm^3 versus $\alpha=2.6\times10^{-24}$ cm^3 for methane[30]).

The amplitude of the baseline subtracted toluene signal [Fig. 9(c)] was 0.1 V at a gain setting of 10^7 V/A, corresponding to 10 nA of current, and the current preamplifier has a rise time of 10 μs. If the rise time (10 μs for the current preamp) is equated to the ion pulse width, 625 000 trapped ions would be expected. If 10 nA was all attributable to trapped ions, this would lead to approximately 3000 ions for a 50 ns pulse width. With all traps in the array populated by 1 or 0 ion (as predicted by simulation[6]), this indicates approximately 15% of the traps being populated each with one ion. However, because the rise time was much longer than the estimated pulse width of about 50 ns, it is hard to deduce the expected number of trapped ions. Since the measured current cannot be all attributed to trapped ions, it is problematic to discern the efficiency of the trap and validate the simulation results.

VII. DISCUSSION

A viable MEMS fabrication process for the microfabrication of micrometer-scale cylindrical ion traps with metallic trap electrodes has been developed. We note that this same fabrication approach is amenable to linear Paul trap configurations as well. The molded tungsten MEMS fabrication process was found to be amenable to fabrication of CITs with air gaps between trap electrodes and cylinder radii of 1, 2, 5, and 10 μm. Ion traps were packaged using a StratEdge glass wall rf flat-pack package. The ion trap array's electrical characteristics were determined and found to provide the minimum trapping conditions necessary for toluene. Although measured signals could not be fully attributed to positive charge, trapping of toluene ions in a massive array of 5 μm internal radius cylindrical ion traps was suggested by the observation of current signals above the noise level upon rf turn off after an ion trapping period. The presence of exposed silicon nitride dielectric on the ion trap chip surface, however, is believed to have caused deleterious build up of negative charge on the trap surface, obfuscating the measurements. Future work should focus on reducing the intrinsic capacitance of the ion trap structures and eliminating exposed dielectric surfaces. While the use of high resistivity silicon suggests the possibility of reducing the capacitance by 30%, the use of degenerately doped silicon, or a metallized substrate, should minimize rf dissipation to the substrate due to the loss tangent. Metallizing the semiconductor substrate on which the traps are built should also accomplish this. Furthermore, a hole through the silicon substrate should provide a further decrease in the intrinsic capacitance, and allow electron injection to, ion ejection from, and optical access into the trapping region. In addition to reducing the number of electrode anchor points which give rise to the voltage drop through the Si substrate, this would enable the flexibility of detecting ions via fluorescence and minimize the electrical noise associated with the signal.

ACKNOWLEDGMENTS

Sandia is a multiprogram laboratory operated by Sandia Corporation, a Lockheed Martin Company, for the United States Department of Energy's National Nuclear Security Administration under Contract DE-AC04-94AL85000. The authors would like to acknowledge technical support by S. Zmuda, the MESA processing teams, the financial support from the MESA Institute, the LDRD Program, and the National Science Foundation (CTS-0329829 and CTS-0319829). One of the authors (D.C.) acknowledges the fellowship support from GEM and UCLA School of Engineering Dean's Fellowship.

[1] W. Paul and H. Steinwedel, Z. Naturforsch. A **8A**, 448 (1953).
[2] W. Paul, Rev. Mod. Phys. **62**, 531 (1990).
[3] P. T. H. Fisk, Rep. Prog. Phys. **60**, 761 (1997).
[4] D. Liebfried, R. Blatt, C. Monroe, and D. Wineland, Rev. Mod. Phys. **75**, 281 (2003).
[5] A. Steane, Appl. Phys. B: Lasers Opt. **64**, 623 (1997).
[6] M. G. Blain, L. S. Riter, D. Cruz, D. E. Austin, G. Wu, W. R. Plass, and R. G. Cooks, Int. J. Mass. Spectrom. **236**, 91 (2004).
[7] D. Cruz, J. P. Chang, and M. G. Blain, Appl. Phys. Lett. **86**, 153502 (2005).
[8] G. E. Patterson, A. J. Guymon, L. S. Riter, M. Everly, J. Griep-Raming, B. C. Laughlin, O. Zheng, and R. G. Cooks, Acta Phys. Univ. Comenianae **74**, 6145 (2002).
[9] L. S. Riter, Y. Peng, R. J. Noll, G. E. Patterson, T. Aggerholm, and R. G. Cooks, Anal. Chem. **74**, 6154 (2002).
[10] O. Kornienko, P. T. A. Reilly, W. B. Whitten, and J. M. Ramsey, Rev. Sci. Instrum. **70**, 3907 (1999).
[11] O. J. Orient, Rev. Sci. Instrum. **73**, 2157 (2002).
[12] W. A. Harris, P. T. A. Reilly, W. B. Whitten, and J. M. Ramsey, Rev. Sci. Instrum. **76**, 064102 (2005).
[13] D. J. Berkeland, Rev. Sci. Instrum. **73**, 2856 (2002).
[14] J. Friedrich, J. Fu, C. L. Hendrickson, and A. G. Marshall, Rev. Sci. Instrum. **75**, 4511 (2004).
[15] S. Pau, C. S. Pai, Y. L. Low, J. Moxom, P. T. A. Reilly, W. B. Whitten, J. M. Ramsey, Phys. Rev. Lett. **96**, 120801 (2006).
[16] E. C. Beaty, J. Appl. Phys. **61**, 2118 (1987).
[17] E. R. Badman and R. G. Cooks, Anal. Chem. **72**, 3291 (2000).

[18] H. G. Dehmelt, Adv. At. Mol. Phys. **3**, 53 (1967).
[19] D. E. Austin, D. Cruz, and M. G. Blain, J. Am. Soc. Mass Spectrom. **17**, 430 (2006).
[20] D. A. Dahl, SIMION, 6.0 ed., Idaho National Engineering and Environmental Laboratory, Idaho Falls, ID, 2000; SIMION, 7.0 ed., Idaho National Engineering and Environmental Laboratory, Idaho Falls, ID, 2000.
[21] Y. Wang, Int. J. Mass Spectrom. Ion Process. **132**, 155 (1994).
[22] W. W. Lee, C. H. Oh, P. S. Kim, M. Yang, and K. Song, Int. J. Mass. Spectrom. **230**, 65 (2003).
[23] P. H. Smith, *Electronic Applications of the Smith Chart in Waveguide, Circuit, and Component Analysis* (Noble, Atlanta, GA, 2000).
[24] J. G. Fleming, S. Y. Lin, I. El-Kady, R. Biswas, and K. M. Ho, Nature (London) **417**, 52 (2002).
[25] V. Milanovic, M. Ozgur, D. C. DeGroot, J. A. Jargon, M. Gaitan, and M. E. Zaghloul, IEEE Trans. Microwave Theory Tech. **46**, 632 (1998).
[26] W. Durr, U. Erben, A. Schuppen, H. Dietrich, and H. Schumacher, IEEE Trans. Microwave Theory Tech. **46**, 712 (1998).
[27] C. Warns, W. Menzel, and H. Schumacher, IEEE Trans. Microwave Theory Tech. **46**, 5 (1998).
[28] NIST Chemistry Webbook, http://webbook.nist.gov
[29] NIST Physical Reference Data, http://physics.nist.gov/PhysRefData/Ionization/
[30] D. R. Lide, *CRC Handbook of Chemistry and Physics*, 84th ed. (CRC, Boca Raton, FL, 2004).